Journal of Materials Chemistry A

Accepted Manuscript

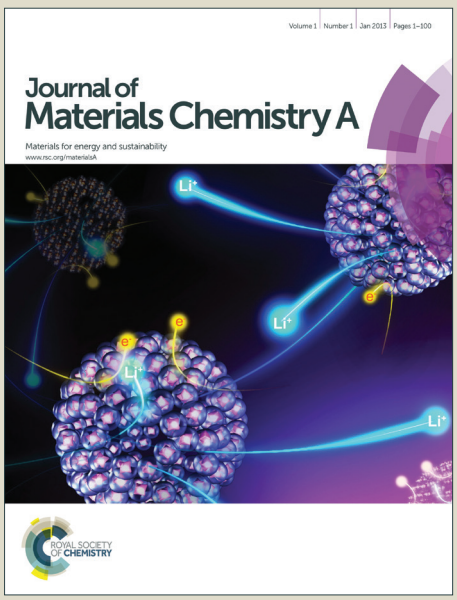

ROYAL SOCIETY OF CHEMISTRY

www.rsc.org/materialsA

Journal Name

RSCPublishing

ARTICLE

Highly regenerable and alkali-resistant magnetic nanoparticles inspired by mussel for smartly selective dye removal toward high-efficiency environmental remediation

VCite this: DOI: 10.1039/x0xx00000x

Received ooth January 2012,
Accepted ooth January 2012

DOI: 10.1039/x0xx00000x

www.rsc.org/

Zhenxing Wang,[a†] Jing Guo,[a†] Jun Ma[b] and Lu Shao[a*]

Most recently, polydopamine (PDA) and its hybrid nanomaterials have been developed as promising adsorbents to remove organic dyes. However, PDA based adsorbents are typically lack of recyclability, alkali resistant and selective adsorption. Herein, novel PDA based magnetic nanoparticles are fabricated for the first time via the simultaneous incorporation of PDA and poly(ethylenimine) (PEI) on Fe_3O_4 nanoparticles simply in one step to overcome almost all disadvantages of "traditional" PDA adsorbents. The constructed PDA based magnetic nanoparticles have ultrathin shell layer (only about 3 nm, much thinner than that of other PDA adsorbents), and can withstand strong alkaline solutions (0.1 M NaOH, pH=13), exhibiting excellent alkali resistance. Remarkably, the nanoparticles show superior performance in smart and fast selective removal (>95%, just in five minutes) of anionic dyes from dye mixtures and can maintain their high efficiency (>90%) even after 10 cycles, indicating the unprecedented selective adsorption capacity and desirable recyclability. The adsorption process follows pseudo-second order reaction kinetics, as well as Langmuir isotherm, indicating that anionic dyes are monolayer adsorbed on the hybrid by electrostatic interaction. In particular, the readily regeneration of the novel composite nanoparticles can be accomplished only within several minutes, demonstrating excellent regeneration ability. Our work can provide new insights into utilizing mussel-inspired materials for environmental remediation and creating advanced magnetic materials for various promising applications.

1. Introduction

Water pollution by organic contaminants has become a serious environmental issue and received widely attention.[1, 2] Among many organic pollutants, organic dyes have already become an important pollutant source in water due to their wide applications in industries and uncontrolled emissions.[3] The direct discharge of wastewater containing organic dyes can lead to serious environmental pollution, and exacerbate water crisis and even harm human beings. Thus diverse technologies have been developed to remove these organic dyes, such as adsorption, membrane filtration, photocatalytic degradation, flocculation, and chemical/electro oxidation.[4-6] Among these methods, adsorption is a promising method because of its effectiveness, relatively low cost and easy operation.[1] A variety of adsorbents have been prepared to remove the dyes in wastewater, such as carbon-based nanomaterials, inorganic materials, and polymer resins.[7-11]

Recently, inspired by the unique wet adhesion capability of marine mussels, polydopamine (PDA) has attracted strong interest as a biomimetic material and surface modification agent for various applications.[12-18] PDA and its hybrid nanomaterials have been developed as novel adsorbents to remove organic dyes, such as PDA microspheres,[19] PDA-graphene composites or hydrogel,[20-22] Fe_3O_4-PDA core-shell microspheres,[23-26] $CaCO_3$-PDA hybrids,[27] electrospun nanofibrous-PDA membranes,[28] and clay-PDA complexes.[29] Despite their considerable adsorption capabilities, most previously reported PDA-based adsorbents are limited by poor alkali resistance, lack of selective adsorption capacity and unsatisfactory recyclability. These drawbacks greatly limit the practical applications of PDA based adsorbents. Most importantly, the poor alkali resistance due to the inherent decomposing property of PDA in strong alkaline solutions will critically deteriorate PDA based absorbents for treating industrial wastewater that is mostly alkaline.[30] On the other hand, the total removal of the compounds is not always required and some valuable chemicals need to be recycled in industrial wastewater from the economical and much practical considerations.[31-33] Thus endowing PDA based materials with selective adsorption capacity have unique usages in the efficiently separation or

recycle of specific target compounds from dye mixtures.[34-36] Recently, Jin et al demonstrated that PDA-GO composite could adsorb dyes selectively.[22] However, the selective process is relative slow and these absorbents are difficult to be recycled, because the selective adsorption mechanism is based on chemical reaction, which may decrease their decontamination efficiencies in dye removal and result in the excessive consumption of absorbents. Therefore, the fabrication of PDA based absorbents capable of fast selective removal of dyes in combination with strong alkaline resistance and favourable regenerability highly desired for practical applications, is toughly challenging.

Herein, for the first time, highly regenerable and strong alkali resistant magnetic composite nanoparticles were fabricated via a novel mussel-inspired strategy with the aid of poly(ethylenimine) (PEI) and applied for efficient selective adsorption of anionic dyes (Fig. 1). Six different dyes including four anionic dyes and two cationic dyes were utilized to evaluate the adsorption performance of our novel particles. The selective adsorption mechanism, the isotherms and kinetics of adsorption process were thoroughly discussed by two model dyes, and the separation efficiency was calculated. Furthermore, the alkali resistance property and regenerability of the magnetic composite nanoparticles were also investigated in detail.

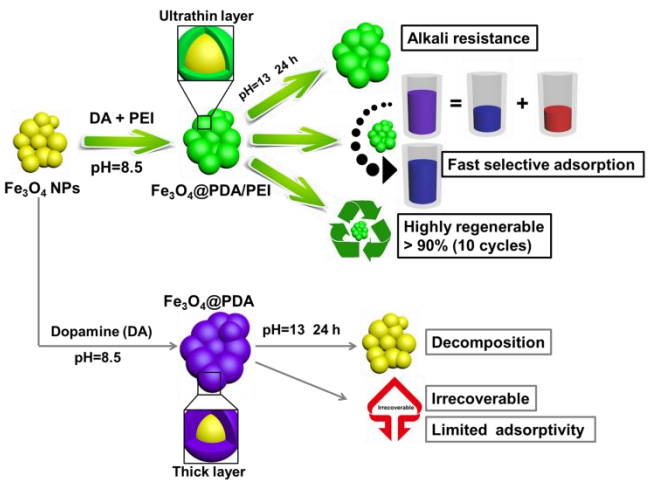

Fig. 1 Schematic of the fabrication and comparison of novel Fe_3O_4@PDA/PEI and Fe_3O_4@PDA magnetic adsorbents.

2. Experimental

2.1 Materials

Dopamine hydrochloride (DA) was purchased from Sigma-Aldrich (USA). Tris(hydroxymethyl)aminomethane (Tris), poly(ethylenimine) (PEI, M_w=600), methylene blue, methyl blue, rose bengal, crystal violet, orange G and amaranths red were obtained from Aladdin (China). Ferric chloride hexahydrate ($FeCl_3 \cdot 6H_2O$), ferrous sulphate heptahydrate ($FeSO_4 \cdot 7H_2O$), ammonium hydroxide (28 wt%), hydrochloric acid (HCl) and anhydrous ethanol were provided by Tianjin Kermel Chemical Reagent Co., Ltd. (China). All the reagents and solvents were used as received without further treatment.

2.2 Synthesis of Fe_3O_4 nanoparticles

Fe_3O_4 nanoparticles were synthesized according to the co-precipitation method with minor modifications.[37] In a typical preparation process, the $FeSO_4 \cdot 7H_2O$ (15.0 g) and $FeCl_3 \cdot 6H_2O$ (25.0 g) were dissolved in deionized water (50 mL) with nitrogen protection under stirring. The mixture solution was heated to 80°C and then $NH_3 \cdot H_2O$ (28 wt%, 50 mL) were added rapidly. The reaction was kept at 80 °C for 3 h. Finally, the mixture was cooled to room temperature. The resultant Fe_3O_4 nanoparticles were washed thoroughly with deionized water and were collected with the aid of a magnet for further modification.

2.3 Synthesis of Fe_3O_4@PDA/PEI composite nanoparticles

Fe_3O_4 (0.2 g) was firstly dispersed in Tris-HCl buffer (pH=8.5, 200 mL) under ultrasonic conditions. Then dopamine (DA, 0.4 g) and poly(ethylenimine) (PEI, M_w=600, 0.6 g) were simultaneously added and allowed to proceed for 24 h under stirring at room temperature. The resulting product named Fe_3O_4@PDA/PEI was separated and collected with a magnet and subsequently washed with deionized water several times and then dried in vacuum at room temperature.

For comparison, pure PDA coated Fe_3O_4 composite nanoparticles were also prepared in the same way without the addition of PEI, and the resultant product was named Fe_3O_4 @ PDA.

2.4 Dye adsorption and renewable experiments

For the dye adsorption, six typical dyes, namely methyl blue, rose bengal, amaranths red, orange G, methylene blue and crystal violet were chosen for the adsorption test. Their chemical structures are shown in Fig.2. For dye adsorption, magnetic composite nanoparticles (10 mg) were added into the dye solution (10 mL) with a certain concentration. The mixture was vibrated continuously for 2 h at room temperature, and then the absorbents were facilely collected and removed with a magnet. The concentration of the residual dye solution was analysed by UV-Vis spectroscopy by measuring the absorbance at the maximum absorption wavelength. The concentrations of each dye before and after adsorption were determined from the standard calibration curve.

For regeneration, the recycled adsorbents were first washed with sodium hydroxide (0.1 M) and then hydrochloric acid (0.1 M), and then were used for the next adsorption process. Note that the whole regeneration process is only several minutes. The above adsorption-desorption cycles were carried out for 10 cycles.

2.5 Alkali-resistance property

The alkali resistance of magnetic composite nanoparticles were evaluated. To test the alkali stability, both the as-prepared Fe_3O_4@PDA/PEI (20 mg) and Fe_3O_4@PDA (20 mg) nanoparticles were dispersed in sodium hydroxide solution (20

mL, pH=13) and shaken for 24 h, respectively. The weight of these nanoparticles and the TEM images before and after alkali treatment were presented to assess the stability of these absorbents.

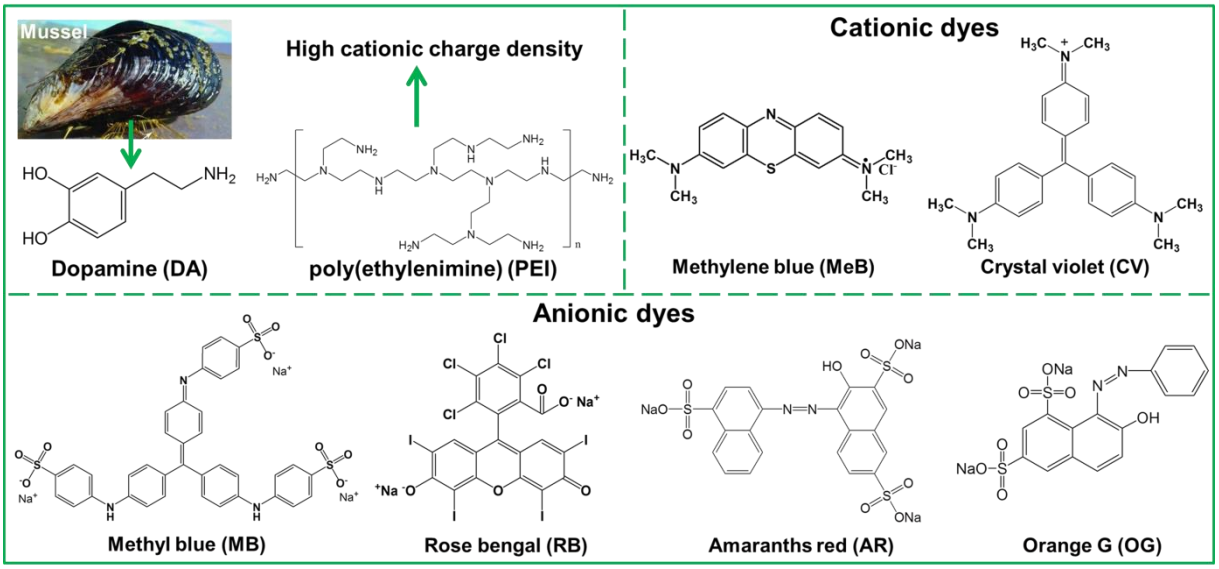

Fig. 2 Molecular structures of dopamine, poly(ethylenimine) (PEI), and the anionic dyes (methyl blue, rose bengal, amaranths red and orange G) and cationic dyes (methylene blue and crystal violet).

2.6 Characterization

The morphologies of Fe_3O_4@PDA and Fe_3O_4@PDA/PEI composite nanoparticles before and after strongly alkali treatment were performed on high resolution transmission electron microscopy (HR-TEM, Tecnai G2 F30, USA). The point of zero charge (PZC) of these microspheres was determined with Zetasizer Nanoseries ZS instrument (Malvern Instruments, United Kingdom). The FTIR measurements were performed using a Spectrum One instrument (Perkin Elmer, USA). XPS analysis was carried out on a Shimadzu AXIS Ultra DLD spectrometer, using an Al Ka X-ray source. All core-level spectra were obtained at a photoelectron take-off angle of 90^o with respect to the sample surface. The TGA curves were determined with a thermal gravimetric analyzer (Q500, TA Instruments, New Castle, DE, USA) over a temperature range from room temperature to 800 ℃ at a heating rate of 10 ℃ min^{-1} under atmosphere.

3. Results and discussion

3.1 Characterizations of materials

The XRD patterns for the magnetic nanoparticles obtained by co-precipitation method (Fig. S1). The peaks at 18.3^o (220), 30.1^o (220), 35.5^o (311), 43.1^o (400), 53.4^o (422), 57.0^o (511), 62.6^o (440) are consistent with the standard date for magnetite, confirming that the obtained magnetic nanoparticles are Fe_3O_4.[37]

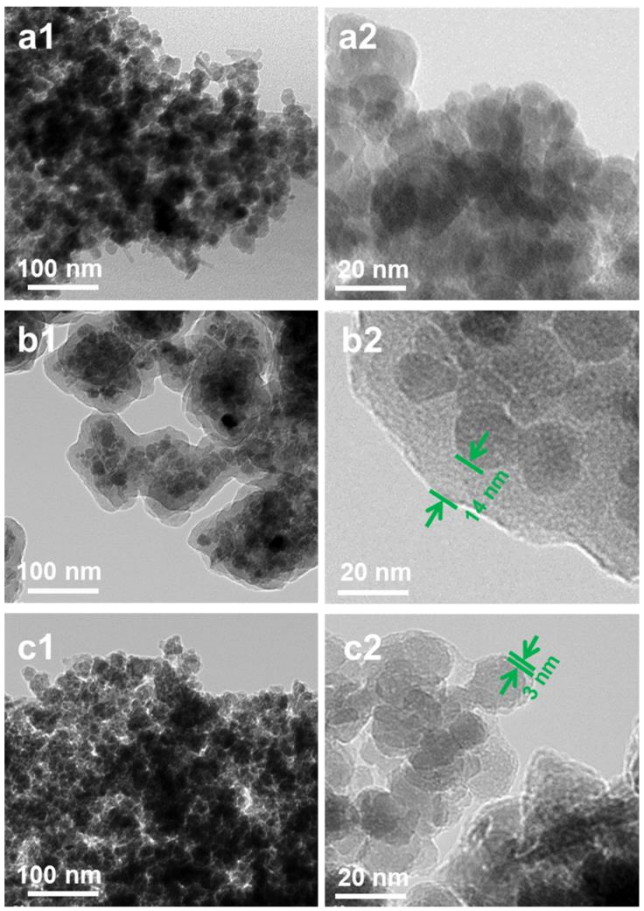

Fig. 3 TEM images of (a) Fe_3O_4, (b) Fe_3O_4@PDA and (c) Fe_3O_4@PDA/PEI composite nanoparticles.

The morphologies of the Fe_3O_4, Fe_3O_4@PDA and Fe_3O_4@PDA/PEI nanoparticles were characterized by TEM (Fig. 3). Obviously, after being treated with either DA or DA/PEI, Fe_3O_4 nanoparticles were coated with layers, forming magnetic composite nanoparticles. Table 1 and Fig. 4a shows the XPS and FTIR results of different magnetic nanoparticles before and after modification. For Fe_3O_4@PDA composite nanoparticles, the new elements of C and N (Table 1), as well as the new peaks at about 1600cm^{-1} attributed to the C=C resonance vibrations in the aromatic ring, indicate the formation of PDA layer. For Fe_3O_4@PDA/PEI nanoparticles, the successful incorporation of PEI in PDA via crosslinking between PDA and PEI can be confirmed by the increased N/C ratio and enhanced peak at 2930 cm^{-1} and 2850cm^{-1} that derived from the C-H stretching vibration absorption (Fig. 4a).[38-41] Interestingly, the addition of PEI can endow the Fe_3O_4@PDA/PEI nanoparticles with ultrathin layer (only about 3 nm) which is much thinner than that of Fe_3O_4@PDA (about 14 nm) and other reported PDA based hybrid adsorbents[23-25]. Yang et al. found that the addition of molecular with abundant amino-group will destroy the noncovalent interactions during the polymerization of dopamine.[40] Most recently, Zuo et al. reported that the addition of PEI could effectively decrease the intra- and intermolecular coupling, and they further found that the destroy or decrease of noncovalent interactions could significantly reduce the size of PDA aggregates.[42] Thus the ultrathin layer on Fe_3O_4@PDA/PEI should be due to the decrease of intra- and intermolecular noncovalent interactions caused by the addition of PEI. Thanks to the ultrathin layer, the Fe_3O_4@PDA/PEI nanoparticles possess much higher BET surface area (29.6 m^2 g^{-1}) than that of Fe_3O_4@PDA composite (17.8 m^2 g^{-1}) (Fig. 4b), which is beneficial for dye absorption.[43]

Table 1 XPS results of elemental composition of different nanoparticles.

Nanoparticles	Composition (At. %)				
	C	N	O	Fe	N/C
Fe_3O_4	/	/	60.2	39.8	/
Fe_3O_4@PDA	74.8	6.0	18.9	0.3	0.08
Fe_3O_4@PDA/PEI	74.0	12.5	13.1	0.4	0.17

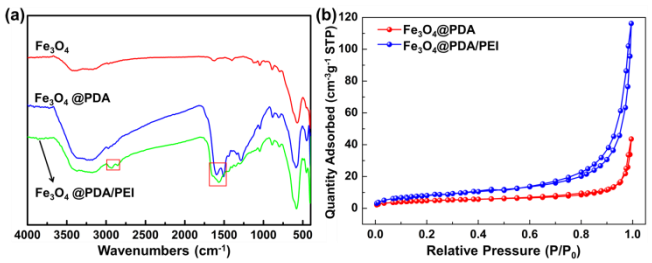

Fig. 4 (a) FTIR spectra of pure Fe_3O_4, Fe_3O_4@PDA, and Fe_3O_4@PDA/PEI composite nanoparticles; (b) Nitrogen absorption/desorption analysis of Fe_3O_4@PDA and Fe_3O_4@PDA/PEI.

3.2 Selective adsorption capacity of the adsorbents

The adsorption performance of the Fe_3O_4@PDA and Fe_3O_4@PDA/PEI with the anionic (methyl blue, rose bengal, amaranths red and orange G) and cationic (methylene blue and crystal violet) dyes (pH=7) were studied and the results are shown in Fig. 5a and Fig. S2. For Fe_3O_4@PDA adsorbents, the adsorption capacities of cationic dyes are only a little higher than that of anionic dyes, disclosing the disheartening selective adsorption capacity. Compared with Fe_3O_4@PDA adsorbents, the as-prepared Fe_3O_4@PDA/PEI nanoparticles display entirely different and exciting adsorption performance: the adsorption capacity of anionic dyes (amaranths red, orange G, methyl blue and rose bengal) are enhanced by 10.8, 11.2, 6.9 and 20.7 times, while the adsorption capacities of cationic (methylene blue and crystal violet) is 8.2 and 9.3 times lower than that of Fe_3O_4@PDA. The distinct opposite effect toward anionic and cationic dyes makes the adsorption capacity of anionic dyes is 30-50 times that of cationic dyes, implying outstanding selectivity of the as-prepared Fe_3O_4@PDA/PEI adsorbent towards anionic dyes. Zeta potentials of the two as-prepared adsorbents disclose the reason for the great changes. As shown in Fig. 5b, the value of pH at which the point of zero charge (PZC) of Fe_3O_4@PDA occurs is around 4.3, while that of Fe_3O_4@PDA/PEI drastically increases to about 9.7. The alteration of PZC not only further confirms the incorporation of cationic PEI on the surface of Fe_3O_4, but also provides a reasonable interpretation for the excellent selectivity toward anionic dyes. When the pH value is about 7, the Fe_3O_4@PDA/PEI surface was protonated to get positive charges due to the incorporation of high charge density cationic PEI and repel the methylene blue and crystal violet that exist as cations, which will lead to the extremely low adsorption of these two dyes. On the contrary, the adsorption capacities of anionic dyes such as methyl blue, rose bengal, amaranths red and orange G are significantly improved due to the strong electrostatic attraction.

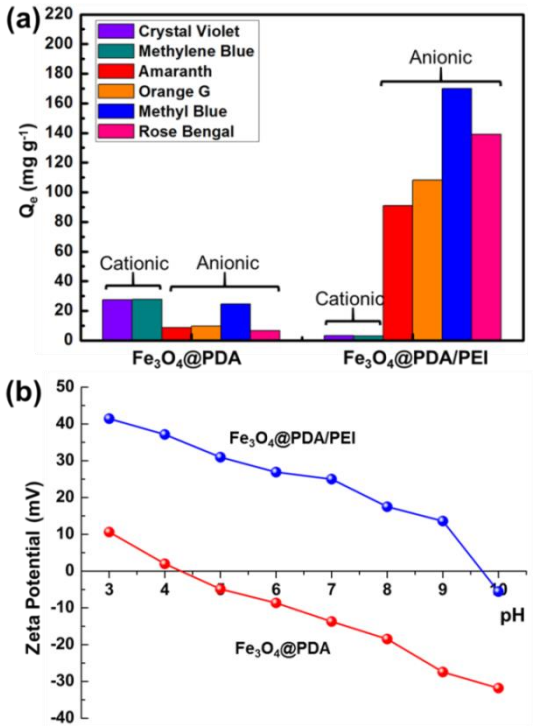

Fig. 5 (a) The adsorption capacity of various cationic and anionic dyes on the as-prepared Fe_3O_4@PDA and Fe_3O_4@PDA/PEI composite nanoparticles at pH=7. (b) Zeta potential at varied pH of Fe_3O_4@PDA and Fe_3O_4@PDA/PEI.

The pH of dye solutions has an important effect on the adsorption process by influencing the surface charges of adsorbents.[6] Thus the effects of pH (from 3 to 9) on the adsorption capacities of Fe_3O_4@PDA/PEI toward anionic methyl blue and cationic methylene blue were further studied, and opposite tendencies were observed (Fig. 6). The lower the pH the higher the adsorption capacity toward methyl blue, while the lower adsorption capacity toward methylene blue. Such effect could be explained by the reinforced protonation of amine and imine groups in PDA/PEI layer under lower pH value, which could be confirmed by the increased zeta potentials of Fe_3O_4@PDA/PEI under lower pH value (Fig. 5b). This process will enhance charge density and thus strengthens the electrostatic interaction between the adsorbents and anionic dye molecules, resulting in the improved adsorption capacity toward methyl blue. Note that the adsorption capacity for anionic methyl blue is almost much higher than that of cationic methylene blue in the range of pH (from 3 to 9). Even if the pH is 9, the adsorption capacity for methyl blue (about 96 mg g^{-1}) is still up to 7 times that for methylene blue (about 13 mg g^{-1}).

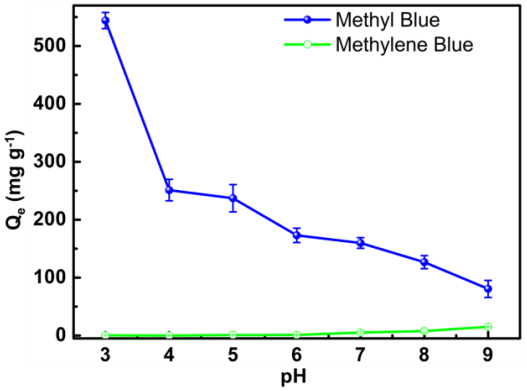

Fig. 6 The effect of pH on the adsorption capacity of Fe_3O_4@PDA/PEI toward methyl blue and methylene blue.

The selective adsorption capacity of the Fe_3O_4@PDA/PEI nanoparticles toward anionic dyes makes them the promising application in separation of anionic dyes from dye mixtures. To exhibit the favorable ability, verification tests were carried out (pH=7). As shown in Fig. 7a-c, three mixed solutions such as OG/CV, RB/MeB and OG/MeB in a 5:1 mass ratio were prepared. Fe_3O_4@PDA/PEI adsorbents were put into the three mixed solutions for certain time to fully adsorb dyes and then collected with the aid of a magnet. It is obviously that the colours of the three mixed solutions change to violet and blue corresponding to the colour of crystal violet and methylene blue respectively, implying the two anionic dyes (OG in mixture-1,3 and RB in mixture-2) are selectively adsorbed onto our novel composite adsorbents. To confirm this point, the UV-Vis spectra of the pristine Mixture-3 and resultant solution was shown in Fig. 6d. Obviously, the absorption peak of OG (478 nm) almost disappears in the resultant solution while there is almost no change for that of MeB (664 nm), demonstrating the orange G is selectively removed from the OG/MeB mixture even though the amount of OG is five times that of the MeB. The separation efficiency for OG in mixture 1 and 2, and RB in mixture 3 was calculated according to

$$(1-\frac{c_1-c_0}{c_0})\times 100\% \qquad (1)$$

Where c_1 and c_0 are the concentration of anionic dye in the solutions before and after selective adsorption.[22] The obtained separation efficiency for OG in Mixture-1, 2 and RB in Mixture-3 are as high as 95.1%, 96.6% and 95.5%, respectively. Notably, the selective separation process can be accomplished just in five minutes, disclosing the high efficiency of our novel adsorbents in wastewater treatment.

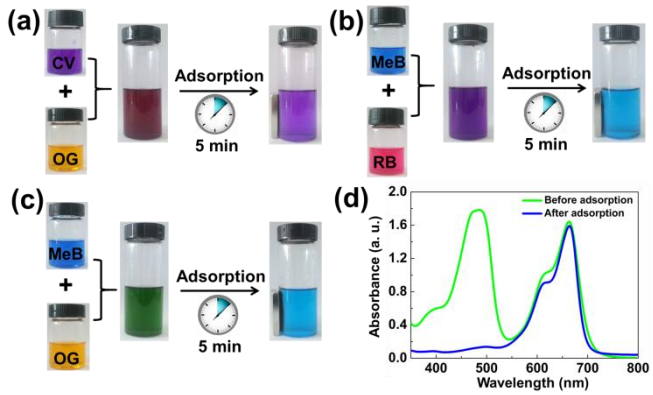

Fig. 7 Photographs of the smart and fast selective adsorption of (a) OG from OG/CV (Mixture-1), (b) RB form RB/MeB (Mixture-2) and (c) OG from OG/MeB (Mixture-3) at pH=7; (d) the UV-Vis spectra of OG/MeB mixture before and after adsorption.

3.3 Adsorption kinetics

As shown in Fig. 8a, the adsorption capacity was enhanced sharply in the initial time, and then slowed down and reached equilibrium finally. Note that forty minutes are enough to attain adsorption equilibrium, which is only about a third of those values for reported PDA based absorbents.[19, 25] The fast adsorption should be attributed to the ultrathin shell and the strong interaction between the cationic ultrathin shell and anionic dyes.[34] Adsorption kinetic studies were thoroughly explored at 25 °C to obtain important information on the adsorption rate and mechanism. Pseudo-second order kinetic model was applied to describe the adsorption of dyes on Fe_3O_4@PDA/PEI, and its linear model was shown below:

$$\frac{t}{q_t} = \frac{1}{kq_e^2} + \frac{t}{q_e} \qquad (2)$$

Where k is the pseudo-second-order rate constant (g mg^{-1} min^{-1}), q_t and q_e is the adsorption capacities of dyes at any and equilibrium time (min), respectively.

As shown in Fig. 8b and Table 2, the fitting curves of pseudo-second order kinetic model exhibits good linearity with R^2 over 0.99. The high k values presented in Table 2 reveal fast adsorption rate of anionic dyes on Fe_3O_4@PDA/PEI adsorbents.

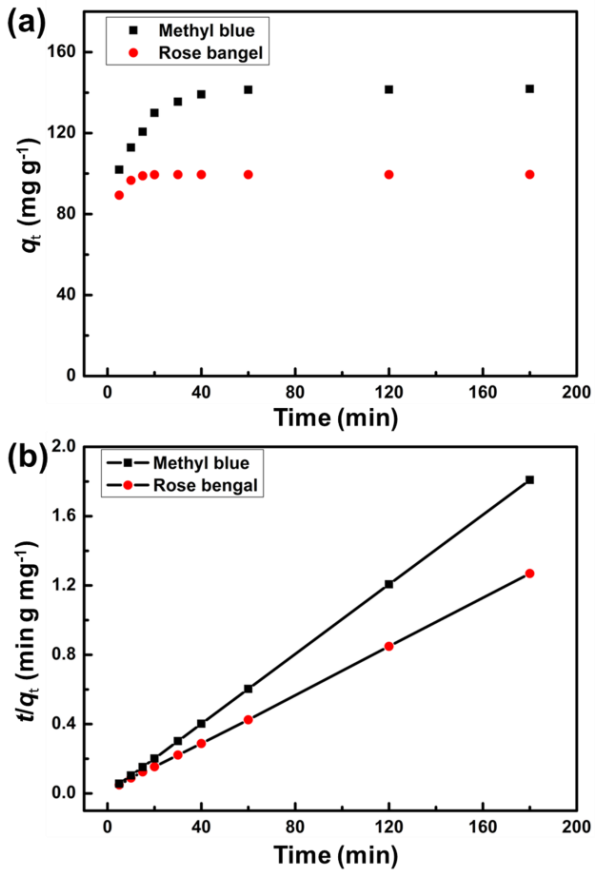

Fig. 8 (a) Adsorption kinetics date of methyl blue and rose bengal on Fe_3O_4@PDA composite nanoparticles at pH=7; (b) curves of pseudo-order kinetic fitting.

Table 2 Pseudo-second-order rate constants for dyes adsorption on Fe_3O_4@PDA/PEI at pH=7.

Dyes	Q_e (mg g^{-1})	k (g mg^{-1} min^{-1})	R^2
Methyl blue	142.85	3.4×10^{-3}	0.9999
Rose bengal	98.03	52.0×10^{-3}	0.9999

3.4 Adsorption isotherms

The adsorption isotherm was carried out at 25 °C. The adsorption data of methyl blue and rose bengal with different concentrations were shown in Fig. 9a. With the rise of dyes concentration, the adsorption capacities increase sharply in the first stage because of the increased driving force derived from the concentration gradient.[22, 25] Two equilibrium isotherm models, Langmuir and Freundlich isotherm models, were applied to analyse the adsorption data of these dyes on Fe_3O_4@PDA/PEI adsorbents, and their linear equations were given below:

$$\frac{c_e}{q_e} = \frac{c_e}{q_0} + \frac{1}{q_0 k_L} \qquad (3)$$

$$\ln q_e = \ln k_F + \frac{1}{n}\ln c_e \qquad (4)$$

Where q_e (mg g^{-1}) and c_e (mg L^{-1}) are the equilibrium adsorption capacity and concentration; q_0 (mg g^{-1}) is the maximum adsorption capacity and k_L (L mg^{-1}) is the equilibrium adsorption constant.

As shown in Fig. 9b, the fitting curves of Langmuir isotherm model exhibite good linearity. According to the two correlation coefficients (R^2) of Langmuir model and Freundlich model shown in Table 3, the obtained data fits well with the Langmuir model rather than Freundlich model, indicating the adsorption of anionic dyes (methyl blue and rose bengal) onto Fe_3O_4@PDA/PEI composite nanoparticles is monolayer adsorption. And the monolayer adsorption capacities for methyl blue and rose bengal calculated from the Langmuir isotherm are 172.4 and 133.3 mg g^{-1}, which approach to the experimental data (170.0 and 139.2 mg g^{-1}).

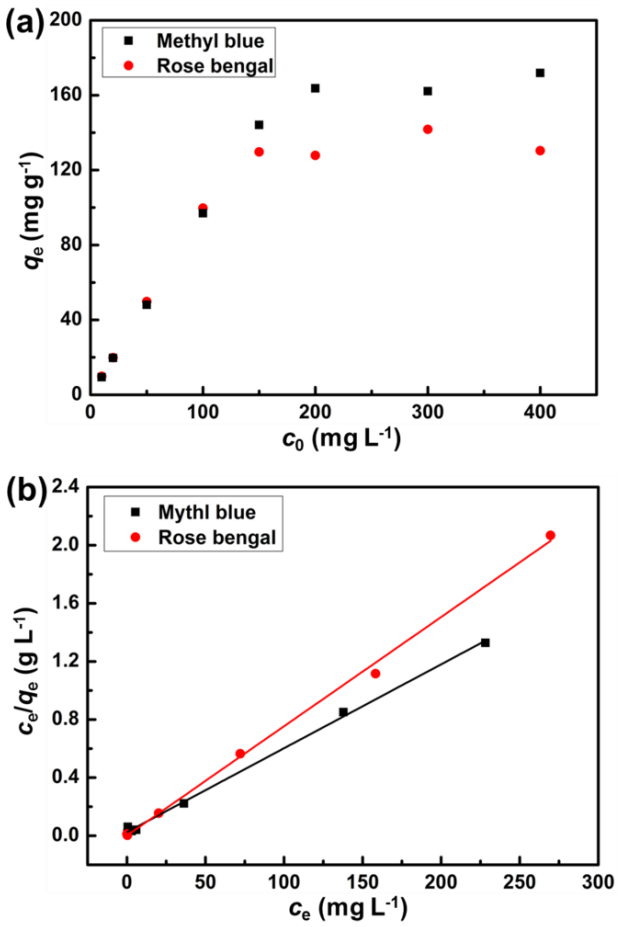

Fig. 9 (a) Adsorption isotherms of mythl blue and rose bengal on Fe_3O_4@PDA/PEI composite nanoparticles at pH=7; (b) fitting curves of Langmuir isotherm models model.

Table 3 Isotherm parameters for methyl blue and rose bengal adsorption on Fe_3O_4@PDA/PEI composite nanoparticles at 298 K (pH=7).

Dyes	Model	Parameters	R^2
Mythyl blue	Langmuir	q_0=172.4 mg g^{-1} k_L=0.23 L mg^{-1}	0.997
	Freundlich	k_F=32.42 n=2.59	0.712
Rose bengal	Langmuir	q_0=133.3 mg g^{-1} k_L=0.38 L mg^{-1}	0.998
	Freundlich	k_F=46.19 n=4.23	0.619

3.5 Recyclability of the adsorbents

The regeneration of the adsorbents was also investigated. Fig. 10 shows that the Fe_3O_4@PDA/PEI composite nanoparticles could be recycled and reused for at least 10 times with a stable adsorption of more than 90%, which is better than the recycle performance of reported PDA based adsorbents[19, 23, 25], Fe_3O_4@C nanocomposites[44] and grapheme or grapheme oxide based hydrogels[20]. Significantly, the regeneration of the Fe_3O_4@PDA/PEI composite nanoparticles can be accomplished only in several minutes, much faster than the regeneration of hydrogel reported previously, which typically lasts more than 30 min.[20]

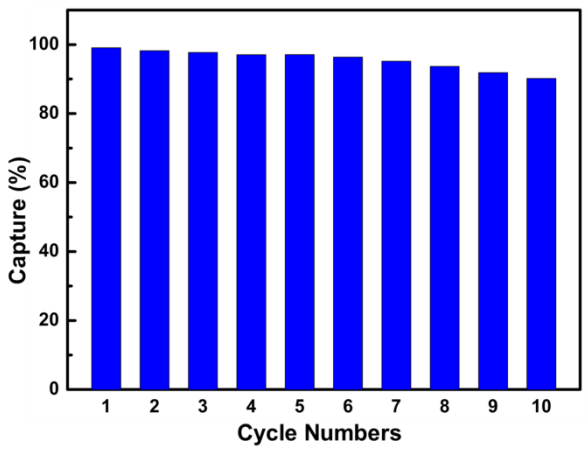

Fig. 10 The recyclability of the Fe_3O_4@PDA/PEI composite nanoparticles for the adsorption of methyl blue.

3.6 Stability of the absorbents

The good stability of adsorbents is a critical factor for their practical applications. It had been reported that PDA cannot withstand strong alkaline solutions and will decompose.[30] Thus the poor alkali resistance is one of the main shortcomings of PDA based adsorbents. In our strategy, the incorporation of strong cationic PEI can endow Fe_3O_4@PDA/PEI nanoparticles with not only desirable selective adsorption capacity and outstanding recyclability, but also the excellent alkali resistance. To demonstrate this prominent feature, both Fe_3O_4@PDA/PEI and Fe_3O_4@PDA were dispersed in strong alkaline solution (pH=13) and shaken for 24 h, and the TGA curves and TEM

images of these adsorbents before and after alkali treatment are provided.

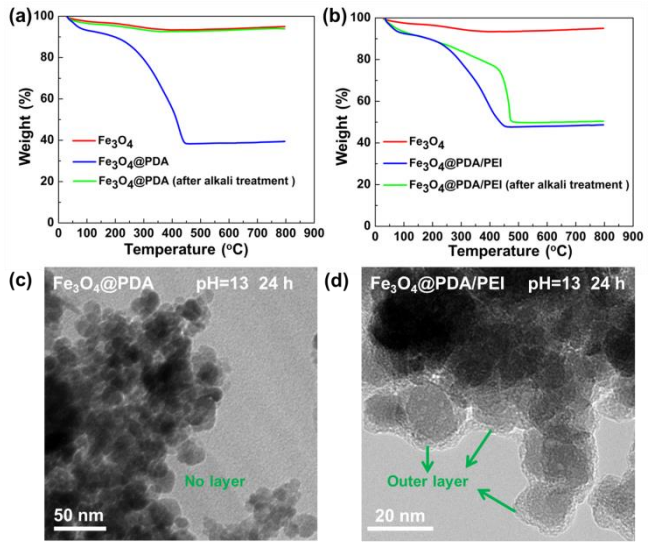

Fig. 11 TEM images of (a) Fe_3O_4@PDA and (b) Fe_3O_4@PDA/PEI nanoparticles after treated by NaOH solution (0.1 M, pH=13) for 24 h; TGA curves of (c) Fe_3O_4@PDA and (d) Fe_3O_4@PDA/PEI before and after alkali treatment (pH=13, 24 h). The TGA curves of pristine Fe_3O_4 nanoparticles are also incorporated in (c) and (d) for comparison.

As shown in Fig. 11a, there is obvious weight loss (about 62%) for Fe_3O_4@PDA due to the thermal decomposition of PDA. Note that, after alkali treatment (pH=13, 24h), the TGA curve of Fe_3O_4@PDA (after alkali treatment) is almost same as that of pure Fe_3O_4. It indicates almost all of PDA coatings on Fe_3O_4@PDA were decomposed during alkali treatment, which can be further confirmed by the disappeared thick shell layer according to the TEM image (Fig. 11c). This phenomenon demonstrates the poor alkali resistance of Fe_3O_4@PDA and is in accordance with other previous report.[30] Jia et al. attributed this phenomenon to the decomposition/destruction of noncovalent interactions in PDA under strongly alkaline solution.[30] Note that when adding PEI in dopamine solution under alkaline solution (pH=8.5), abundant covalent interactions in/between PDA aggregations will be generated because of the Michael addition reactions between amines in PEI and catechol moieties in dopamine or PDA[12]. According to Jia's speculate (the poor alkali resistance of PDA was due to the decomposition/destruction of noncovalent interactions in PDA under strongly alkaline solution), the introduction of covalent interactions in/between PDA aggregations that were originally formed through noncovalent will no doubt improve the alkali resistance of PDA based materials. As expected, the Fe_3O_4@PDA/PEI adsorbents did exhibit desirable alkali resistance. As shown in Fig. 11 b, the weight loss (about 50%) of Fe_3O_4@PDA/PEI (after alkali treatment) is only a little less than that of Fe_3O_4@PDA/PEI (53%). This indicates only a little amount of PDA/PEI was decomposed during the alkali treatment, which can be further proved by the still clearly visible ultrathin shell (Fig.11d), disclosing the excellent alkali resistance of the ultrathin shell of our novel adsorbents. These results further indicate the poor alkali resistance of PDA is due to the decomposition of noncovalent interactions in PDA, and the introduction of abundant covalent interactions will effectively and significantly improve the alkali resistance of PDA based materials.

4. Conclusions

In conclusion, novel magnetic PDA based adsorbents are fabricated via the co-deposition of PDA and PEI onto Fe_3O_4 nanoparticles. The incorporation of PEI during the self-polymerization of dopamine offers several distinct advantages. Firstly, the incorporation of PEI is conducive to constructing ultrathin PDA/PEI layer (only about 3 nm, much thinner than that of pure PDA coating) on Fe_3O_4 particles, which is beneficial to enhance the adsorption capacity due to the increased BET surface. Secondly, the resultant Fe_3O_4@PDA/PEI adsorbents eliminate the inherent poor alkali resistance of PDA based adsorbents because of the crosslinking between PEI and PDA in one step, and can withstand strong alkali (pH=13). Thirdly, due to the high cationic charge density of PEI, the Fe_3O_4@PDA/PEI adsorbents can fast and selectively adsorb cationic dyes from mixed dyes via electrostatic interaction, and the separation efficiency can up to 95%. Notably, the adsorbents can maintain their high efficiency (>90%) even after 10 cycles, and the regeneration process can be accomplished only within several minutes, showing desirable and fast regeneration ability. The adsorption process for anionic dyes follows pseudo-second order reaction kinetics, as well as Langmuir isotherm, indicating that anionic dyes are monolayer adsorbed on the hybrid by electrostatic interaction. The novel Fe_3O_4@PDA/PEI adsorbents with excellent alkali resistance, desirable selective adsorption ability, and high-efficiency recyclability exhibit favourable and unique flexibility and potentials in dye wastewater treatment.

Acknowledgements

This work was supported by National Natural Science Foundation of China (U1462103, 21177032, 51378141), Program for New Century Excellent Talents in University (NCET-11-0805), the Fundamental Research Funds for the Central Universities (Grant No. HIT.BRETIV.201307), Harbin Science and Technology Innovation Talent Funds (2014RFXXJ028) and State Key Laboratory of Urban Water Resource and Environment (Harbin Institute Technology) (No. 2014DX05).

Notes and references

[a] School of Chemical Engineering and Technology, State Key Laboratory of Urban Water Resource and Environment (SKLUWRE), Harbin Institute of Technology, Harbin 150001, PR China.
[b] Harbin Institute of Technology, School of Municipal and Environmental Engineering, State Key Laboratory of Urban Water Resource and Environment (SKLUWRE), Harbin 150001, PR China.
† These authors contributed equally to this work.

Electronic Supplementary Information (ESI) available: XRD patterns of magnetic nanoparticles fabricated by co-precipitation method, photo images of six different dyes before and after adsorption with Fe_3O_4@PDA/PEI. See DOI: 10.1039/b000000x/

1. I. Ali, *Chem. Rev.*, 2012, **112**, 5073-5091.
2. M. M. Khin, A. S. Nair, V. J. Babu, R. Murugan and S. Ramakrishna, *Energy Environ. Sci.*, 2012, **5**, 8075-8109.
3. L. Shao, X. Cheng, Z. Wang, J. Ma and Z. Guo, *J. Membr. Sci.*, 2014, **452**, 82-89.
4. Y. P. Tang, J. X. Chan, T. S. Chung, M. Weber, C. Staudt and C. Maletzko, *J. Mater. Chem. A*, 2015, **3**, 10573-10584.
5. S. Zhang, G. Qiu, Y. P. Ting and T.-S. Chung, *Colloids Surf. A*, 2013, **436**, 207-214.
6. W.-Z. Qiu, H.-C. Yang, L.-S. Wan and Z.-K. Xu, *J. Mater. Chem. A*, 2015, **3**, 14438-14444.
7. F. Perreault, A. Fonseca de Faria and M. Elimelech, *Chem. Soc. Rev.*, 2015. DOI: 10.1039/c5cs00021a
8. S. K. Kansal and A. Kumari, *Chem. Rev.*, 2014, **114**, 4993-5010.
9. M. Khajeh, S. Laurent and K. Dastafkan, *Chem. Rev.*, 2013, **113**, 7728-7768.
10. M.-M. Titirici, R. J. White, C. Falco and M. Sevilla, *Energy Environ. Sci.*, 2012, **5**, 6796-6822.
11. M. E. Calvo, S. Colodrero, N. Hidalgo, G. Lozano, C. López-López, O. Sánchez-Sobrado and H. Míguez, *Energy Environ. Sci.*, 2011, **4**, 4800-4812.
12. H. Lee, S. M. Dellatore, W. M. Miller and P. B. Messersmith, *Science*, 2007, **318**, 426-430.
13. L. Shao, Z. X. Wang, Y. L. Zhang, Z. X. Jiang and Y. Y. Liu, *J. Membr. Sci.*, 2014, **461**, 10-21.
14. Z.-X. Wang, C.-H. Lau, N.-Q. Zhang, Y.-P. Bai and L. Shao, *J. Mater. Chem. A*, 2015, **3**, 2650-2657.
15. Y. Liu, K. Ai and L. Lu, *Chem. Rev.*, 2014, **114**, 5057-5115.
16. Z. Wang, X. Jiang, X. Cheng, C. H. Lau and L. Shao, *ACS Appl. Mater. Interfaces*, 2015, **7**, 9534-9545.
17. H.-C. Yang, J.-Q. Luo, Y. Lv, P. Shen and Z.-K. Xu, *J. Membr. Sci.*, 2015, **483**, 42-59.
18. Z. Wang, Y. Xu, Y. Liu and L. Shao, *J. Mater. Chem. A*, 2015, **3**, 12171-12178.
19. J. Fu, Z. Chen, M. Wang, S. Liu, J. Zhang, J. Zhang, R. Han and Q. Xu, *Chem. Eng. J.*, 2015, **259**, 53-61.
20. H. Gao, Y. Sun, J. Zhou, R. Xu and H. Duan, *ACS Appl. Mater. Interfaces*, 2013, **5**, 425-432.
21. C. Cheng, S. Li, J. Zhao, X. Li, Z. Liu, L. Ma, X. Zhang, S. Sun and C. Zhao, *Chem. Eng. J.*, 2013, **228**, 468-481.
22. Z. Dong, D. Wang, X. Liu, X. Pei, L. Chen and J. Jin, *J. Mater. Chem. A*, 2014, **2**, 5034-5040.
23. R. Liu, Y. Guo, G. Odusote, F. Qu and R. D. Priestley, *ACS Appl. Mater. Interfaces*, 2013, **5**, 9167-9171.
24. Y. Xie, B. Yan, H. Xu, J. Chen, Q. Liu, Y. Deng and H. Zeng, *ACS Appl. Mater. Interfaces*, 2014, **6**, 8845-8852.
25. S. Zhang, Y. Zhang, G. Bi, J. Liu, Z. Wang, Q. Xu, H. Xu and X. Li, *J. Hazard. Mater.*, 2014, **270**, 27-34.
26. X. Han, L. Zhang and C. Li, *RSC Adv.*, 2014, **4**, 30536-30541.
27. C. Li, Z.-j. Qian, C. Zhou, W. Su, P. Hong, S. Liu, L. He, Z. Chen and H. Ji, *RSC Adv.*, 2014, **4**, 47848-47852.
28. J. Yan, Y. Huang, Y. E. Miao, W. W. Tjiu and T. Liu, *J. Hazard. Mater.*, 2015, **283**, 730-739.
29. S. Huang, L. Yang, M. Liu, S. L. Phua, W. A. Yee, W. Liu, R. Zhou and X. Lu, *Langmuir*, 2013, **29**, 1238-1244.
30. H. Wei, J. Ren, B. Han, L. Xu, L. Han and L. Jia, *Colloids Surf. B*, 2013, **110**, 22-28.
31. N. Cheng, Q. Hu, Y. Guo, Y. Wang and L. Yu, *ACS Appl. Mater. Interfaces*, 2015, **7**, 10258-10265.
32. X. Liu, L. Yan, W. Yin, L. Zhou, G. Tian, J. Shi, Z. Yang, D. Xiao, Z. Gu and Y. Zhao, *J. Mater. Chem. A*, 2014, **2**, 12296-12303.
33. S.-D. Pan, H.-Y. Shen, L.-X. Zhou, X.-H. Chen, Y.-G. Zhao, M.-Q. Cai and M.-C. Jin, *J. Mater. Chem. A*, 2014, **2**, 15345-15356.
34. R. Wang, B. Yu, X. Jiang and J. Yin, *Adv. Funct. Mater.*, 2012, **22**, 2606-2616.
35. H. Chen, X. Wang, J. Li and X. Wang, *J. Mater. Chem. A*, 2015, **3**, 6073-6081.
36. L. Lu, X. Yue, F. Lin, F. Huang, B. Zhang and Z. Lin, *J. Mater. Chem. A*, 2015, **3**, 10959-10968.
37. T. Gong, D. Yang, J. Hu, W. Yang, C. Wang and J. Q. Lu, *Colloids Surf. A*, 2009, **339**, 232-239.
38. Y. Tian, Y. Cao, Y. Wang, W. Yang and J. Feng, *Adv. Mater.*, 2013, **25**, 2980-2983.
39. S. Hong, C. F. Schaber, K. Dening, E. Appel, S. N. Gorb and H. Lee, *Adv. Mater.*, 2014, **26**, 7581-7587.
40. H.-C. Yang, K.-J. Liao, H. Huang, Q.-Y. Wu, L.-S. Wan and Z.-K. Xu, *J. Mater. Chem. A*, 2014, **2**, 10225-10230.
41. L. Shao, Y.-P. Bai, X. Huang, L.-H. Meng and J. Ma, *J. Appl. Polym. Sci.*, 2009, **113**, 1879-1886.
42. C. Zhao, F. Zuo, Z. Liao, Z. Qin, S. Du and Z. Zhao, *Macromol. Rapid Commun.*, 2015, **36**, 909-915.
43. G. Lian, X. Zhang, S. Zhang, D. Liu, D. Cui and Q. Wang, *Energy Environ. Sci.*, 2012, **5**, 7072-7080.
44. M. Zhu, C. Wang, D. Meng and G. Diao, *J. Mater. Chem. A*, 2013, **1**, 2118-2125.